Chemical Engineering Science 158 (2017) 445–452

Contents lists available at ScienceDirect

Chemical Engineering Science

journal homepage: www.elsevier.com/locate/ces

Modelling of artefacts in estimations of particle size of needle-like particles from laser diffraction measurements

Okpeafoh S. Agimelen[a,*], Anthony J. Mulholland[b], Jan Sefcik[a,*]

[a] EPSRC Centre for Innovative Manufacturing in Continuous Manufacturing and Crystallisation, Department of Chemical and Process Engineering, University of Strathclyde, James Weir Building, 75 Montrose Street, Glasgow G1 1XJ, United Kingdom

[b] Department of Mathematics and Statistics, University of Strathclyde, Livingstone Tower, 26 Richmond Street, Glasgow G1 1XH, United Kingdom

ARTICLE INFO

Keywords:
Particle size distribution
Particle shape
Particle sizing
Light scattering
Laser diffraction

ABSTRACT

Manufacturing of particulate products across many industries relies on accurate measurements of particle size distributions in dispersions or powders. Laser diffraction (or small angle light scattering) is commonly used, usually off-line, for particle size measurements. The estimation of particle sizes by this method requires the solution of an inverse problem using a suitable scattering model that takes into account size, shape and optical properties of the particles. However, laser diffraction instruments are usually accompanied by software that employs a default scattering model for spherical particles, which is then used to solve the inverse problem even though a significant number of particulate products occur in strongly non-spherical shapes such as needles. In this work, we demonstrate that using the spherical model for the estimation of sizes of needle-like particles can lead to the appearance of artefacts in the form of multimodal populations of particles with size modes much smaller than those actually present in the sample. This effect can result in a significant under-estimation of the mean particle size and in false modes in estimated particles size distributions.

1. Introduction

Particle size measurements are crucial across many industries in the manufacturing of particulate products, such as pharmaceuticals, agrochemicals, detergents, pigments and food. Particle size and shape have a profound influence on downstream processing as well as on final product properties through a variety of product attributes, such as solubility, dissolution kinetics, flowability, etc. There are various particles sizing methods commonly employed in practice, some of them online and others offline (Washington, 1992; Shekunov et al., 2007; Abbireddy and Clayton, 2009). One of the widely used techniques for measuring of particle size distribution (PSD) in dispersions is laser diffraction (Black et al., 1996) which is typically arranged in a flow-through setting but is most often used off line as there are limits on dispersion densities due to multiple scattering. Laser diffraction measurement involves the collection of scattered light from a dilute dispersion of particles by an array of detectors placed at different spatial locations so that they cover a certain span of scattering angles θ. Since the angular dependence of the scattered light intensity originating from a particle is a function of the size and shape of the particle, as well as the orientation of the particle with respect to the incident laser beam, the particle size and shape can be inferred from the corresponding scattering intensity pattern. However, as there is typically a distribution of particle sizes across a population, the intensity pattern measured by the detectors will be a convolution of the intensity patterns from all the particles of different sizes in the dispersion.

The estimation of the PSD from the measured scattering intensity pattern (scattering intensity as a function of scattering angle) involves solving an inverse problem using a suitable scattering model which describes the scattering intensity for particles of a given shape, size and optical properties. The inversion is implemented in the software accompanying laser diffraction instruments, typically using the Mie scattering model (Bohren and Huffman, 1983) for spherical particles as a default, regardless of the shape of particles in the measured sample. This can lead to various artefacts, such as apparently multimodal distributions in PSD estimates (e.g., Hamilton et al., 2012; Polakowski et al., 2014) when the shape of the particles in the sample deviates significantly from spherical. This could result in misleading estimates of mean particles sizes with severe consequences for applications where the process is very sensitive to the particle sizes. This is particularly important in the pharmaceutical industry where many of the active pharmaceutical ingredients are crystallised in needle-like habits.

In this paper, we demonstrate that multimodal PSDs can be obtained from the inversion process even when the true particle size

* Corresponding authors.
E-mail addresses: okpeafoh.agimelen@strath.ac.uk (O.S. Agimelen), jan.sefcik@strath.ac.uk (J. Sefcik).

http://dx.doi.org/10.1016/j.ces.2016.10.031
Received 14 July 2016; Received in revised form 23 September 2016; Accepted 17 October 2016
Available online 18 October 2016

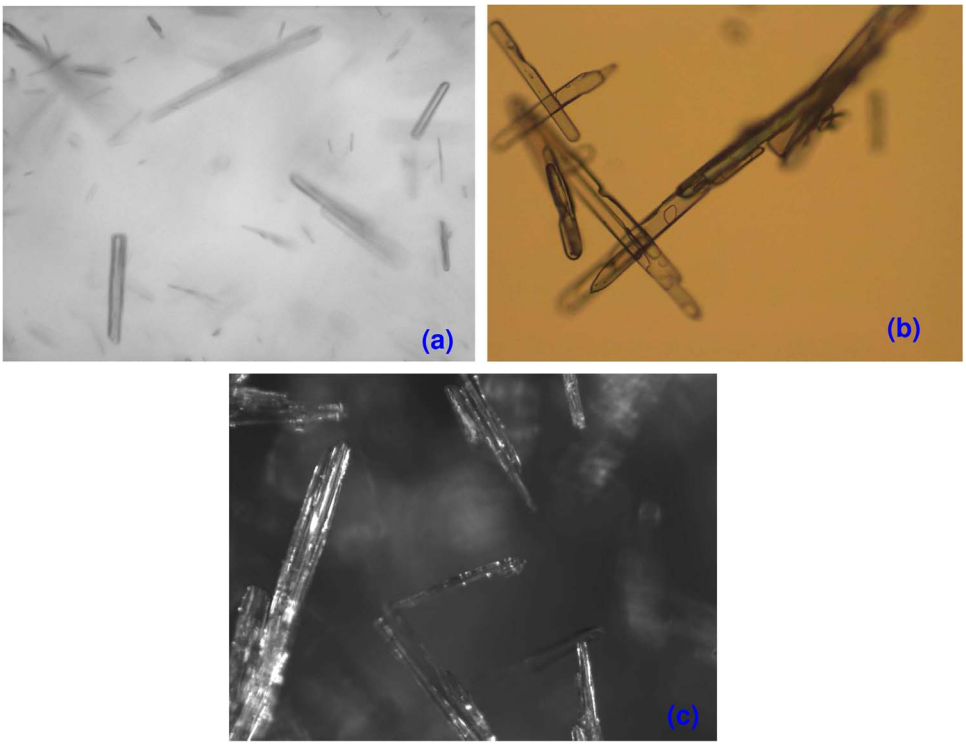

Fig. 1. Images of typical needle-like crystals of (a) cellobiose octaacetate, (b) benzoic acid and (c) metformin hydrochloride.

is monodisperse, i.e., all particles are of the same size. We simulate the scattering intensity patterns for monodisperse population of needle-like particles to explain how multimodal PSD artefacts arise due to solving the inverse problem using a scattering model for spherical particles. We compute the angularly dependent scattering intensity for needle-like particles of specified optical properties using a model for infinitely long cylinders with diameters ranging from 1 to 100 micrometres. Then we solve the inverse problem of estimating PSD from the angularly dependent scattering intensity pattern using the Mie theory for spherical particles, mimicking the analysis performed when using commercial laser diffraction instruments. Since the PSD of needle-like particles is exactly specified here, the estimated PSD from the inversion can be directly compared with the actual PSD. We consider two limiting cases, when needle-like particles are assumed to perfectly aligned with flow which is perpendicular to the incident laser beam and when they adopt random orientations. We show that in either case the inversion results in estimated PSD that are multimodal where smaller modes are mathematical artefacts due to inversion and we explain how these are related to different shapes of intensity scattering patterns for needle-like particles compared to those of spheres.

2. Calculating scattering intensity

The scattering intensity patterns for needle-like particles will be simulated using the scattering theory for infinitely long cylinders (Bohren and Huffman, 1983). Even though the theory was developed for infinitely long cylinders, it is applicable for needle-like particles with lengths significantly larger than their diameters (Wickramasinghe, 1973). Such long thin particles of approximately cylindrical shape are similar to needle-like particles often encountered in pharmaceutical and chemical manufacturing. For example, in Fig. 1 we show typical particles of cellobiose octaacetate, benzoic acid and metformin hydrochloride. As needle-like particles are modelled as infinitely long cylinders in this work, the circular cross-sectional diameters of these cylinders will be used to represent the size of needle-like particles as their length cannot be specified. The scattering intensity pattern for spherical particles will be simulated using the Mie theory (see Bohren and Huffman, 1983 and Section 1 of the supplementary information for details). The procedure for performing the calculations is described below.

Consider a detector system (Fig. 2(a)) in which a monochromatic light with wave vector $\mathbf{k}_i$ is incident on a particle of arbitrary size and shape. The scattered light with wave vector $\mathbf{k}_s$ is then collected at different angles θ to the direction of propagation of the incident light by an array of detectors as depicted in Fig. 2(a). Both the incident and scattered light have components parallel and perpendicular to the scattering plane (the plane containing the incident and scattered light) (Bohren and Huffman, 1983). The scattering wave vector $\mathbf{q}$ is the difference between the incident and scattered wave vectors as sketched in Fig. 2(b). The magnitude of the scattering wave vector is a function of the scattering angle θ, and it is given by Sorensen (2001)

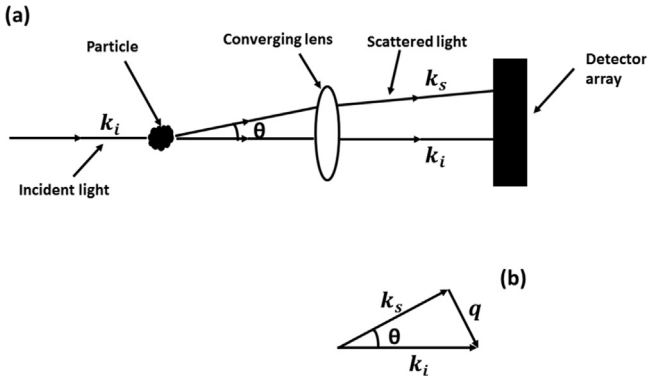

Fig. 2. (a) Schematic of the setup of typical laser diffraction instruments. (b) Illustration of the scattering wave vector.

$$q = \frac{4\pi}{\lambda}\sin(\theta/2), \tag{1}$$

where λ is the wavelength of the incident light. The wavelength of $\lambda = 0.633\ \mu m$ was used in all calculations in this work consistent with the wavelength of red light in typical commercial laser diffraction instruments.

The intensity of the scattered light $\mathbf{I}$ (which is a function of the scattering angle θ) is related to the intensity of the incident light $\mathbf{I}_0$ by means of the phase or scattering matrix $\mathbf{Z}$ as Bohren and Huffman (1983), Mishchenko et al. (2000) (see also Section 1 of the supplementary information for details)

$$I(q_j) = \frac{I_0}{k^2 r^2}\sum_{i=1}^{N} Z_{11}(q_j, \overline{D}_i)X(\overline{D}_i). \tag{2}$$

where the magnitude of the wave vector q has been discretised[1] into $j = 1, 2\ldots,M$ angular positions. The particle size (represented by diameter of spherical or circular cross section of needle-like particles modelled as infinitely long cylinders in this work) D_i, $i = 1, 2,\ldots,N$ has been discretised into N particle size classes[2] such that the characteristic diameter $\overline{D}_i$ of particles whose diameters lie between D_i and D_{i+1} is given by $\overline{D}_i = \sqrt{D_i D_{i+1}}$. The number of particles whose diameters lie between D_i and D_{i+1} is given by $X(\overline{D}_i)$. Finally, the quantity $Z_{11}(q_j, \overline{D}_i)$ is the first component (see Section 1 of the supplementary information) of the phase matrix averaged over particles whose sizes lie between D_i and D_{i+1}.

Writing $I(q_j)$ as I_j, $Z_{11}(q_j, \overline{D}_i)$ as $\widetilde{Z}_{j,i}$ and $X(\overline{D}_i)$ as X_i, then Eq. (2) can be written as a matrix equation as

$$I_j = \mathbf{I} = \frac{I_0}{k^2 r^2}\sum_{i=1}^{N}\widetilde{Z}_{j,i}X_i = \frac{I_0}{k^2 r^2}\widetilde{\mathbf{Z}}\mathbf{X}. \tag{3}$$

The scaling factor in Eq. (3) can be removed if the scattering intensity is rescaled by the scattering intensity I_1 measured at an angular position close to zero. That is, the zero q limit of the scattering intensity. The choice of I_1 for rescaling the scattering intensity is reasonable since the quantity Z_{11} assumes a flat profile at the zero q limit for particles of different shapes and sizes and refractive indices (Bohren and Huffman, 1983). If the first detector in the array of detectors (Fig. 1) is placed at an angular position sufficiently close to zero, then the scattering intensity at the zero q limit for the particles in the N size classes can be constructed from the first row of matrix $\widetilde{\mathbf{Z}}$ as

$$I_1 = \frac{I_0}{k^2 r^2}\sum_{i=1}^{N}\widetilde{Z}_{1,i}X_i. \tag{4}$$

Then the rescaled scattering intensity $\tilde{\mathbf{I}}_j$ can be constructed as

$$\tilde{I}_j = \frac{I_j}{I_1} = \frac{\sum_{i=1}^{N}\widetilde{Z}_{j,i}X_i}{\sum_{i=1}^{N}\widetilde{Z}_{1,i}X_i}. \tag{5}$$

[1] The values of scattering angles $\theta = 0.0015°$ to $\theta = 180°$ were used in all the calculations in this work. This is to ensure that the entire forward direction for scattering is covered. The quantity $1/q$ has the dimension of length, and it sets the length scale accessible in a light scattering experiment (Sorensen, 2001). The smallest and largest values of θ correspond to length dimensions $1/q$ of order 3800μm and 0.05μm respectively. These are the same order of magnitude as the largest and smallest particle diameters of $D_{N+1} = 3500\ \mu m$ and $D_1 = 0.01\ \mu m$ (respectively) in the particle size grid used in the calculations. The angular positions θ were discretised on a geometrically spaced grid with 100 bins. This then gives a size difference of order $L^2\Delta q\ \mu m$ (where L is an arbitrary particle size and Δq is the q spacing). As low q ($\Delta q \approx 10^{-4}\ \mu m^{-1}$) values correspond to large particle sizes, then using $L = 3800\ \mu m$ gives a size difference of 144μm, which is about 4% of D_{N+1}. This is the resolution of the largest particle size. In the large q ($\Delta q \approx 1\ \mu m^{-1}$) region, which corresponds to small particles, the size difference is of order $10^{-4}\ \mu m$ (using $L = 0.01\ \mu m$) which is about 1% of D_1, and this is the resolution of the smallest particle size.

[2] A particle size grid with N=200 size classes was used in the calculations here. The particle diameters on the grid run from $D_1 = 0.01\ \mu m$ to $D_{N+1} = 3500\ \mu m$. This covers the entire range of particle diameters in typical commercial laser diffraction instruments.

The rescaled scattering intensity in Eq. (5) is the form in which the scattering intensity data is reported in typical commercial laser diffraction instruments. Hence this form of the scattering intensity will be used in subsequent analysis in this work. The components of the phase matrix take different forms depending on the shape of the particles (see Section 1 of the supplementary information).

3. Forward and inverse problems

In a dispersion of particles of different sizes, the scattering intensity $\tilde{\mathbf{I}}^*$ that is measured will be a convolution of the scattering intensities of the individual particles in the dispersion and the PSD $\mathbf{X}$ given by Eq. (2). If the PSD $\mathbf{X}$ of the particles in the dispersion is given, then the scattering intensity of the population can be calculated by solving the forward problem in Eq. (5). The calculated scattering intensity $\tilde{\mathbf{I}}$ can then be compared with the measured scattering intensity.

In reality the PSD $\mathbf{X}$ of the particles in a dispersion will not be known. Instead the challenge will be to estimate the PSD corresponding to a measured scattering intensity. This will involve solving an inverse problem. As mentioned earlier, the purpose of this work is to examine the effect of the model employed in solving the inverse problem on the solutions obtained. To achieve this objective, the experimentally measured scattering intensity $\tilde{\mathbf{I}}^*$ will be simulated with the model for infinitely long cylinders. The scattering intensity $\tilde{\mathbf{I}}$ calculated using the model for spherical particles (see Section 1 of the supplementary information for details) will then be used to fit a given simulated intensity $\tilde{\mathbf{I}}^*$.

In this work, the inversion required to obtain the PSD $\mathbf{X}$ will be carried out by minimising the objective function f given as

$$f = \sum_{j=1}^{M} w_j[\tilde{I}_j^* - \tilde{I}_j]^2, \tag{6}$$

This is a weighted least square problem which is an unconstrained optimisation problem (Boyd and Vandenberghe, 2004). The weight function w_j is given as

$$w_j = \frac{1}{1 + |C_1|\tilde{I}_j + |C_2|\tilde{I}_j^2}, \tag{7}$$

where the quantities C_1 and C_2 are optimisation parameters with initial values $C_1 = C_2 = 0$. The weighting function in the objective function in Eq. (6) is necessary as the values of the scattering intensity cover several orders of magnitude over the entire q range of interest. A similar weighting function was employed previously (Schenk et al., 1998) for the calculation of intensity for anti-Stokes Raman scattering but with fixed values of C_1 and C_2.

3.1. Number and volume based PSD

The PSD defined in Eq. (5) which is calculated by solving the least square problem in Eq. (6) is number based. The number based PSD X_i is defined as an exponential function of the parameter γ_i as[3]

$$X_i = e^{\gamma_i}, \quad i = 1, 2,\ldots,N. \tag{8}$$

Then the optimisation problem given in Eq. (6) is solved by searching for γ_i (using the Levenberg–Marquardt algorithm as implemented in Matlab) which minimises the objective function f given in Eq. (6). As the Levenberg–Marquardt method is gradient based and the objective function in Eq. (6) contains local minima, then a multi-start strategy (Aster et al., 2013) is used to search for a solution which is close to the global minimum. Once a solution close to the global minimum is found,

[3] The formulation of the PSD as an exponential function with the free parameter γ ensures that the PSD is non negative and free to assume any shape. A prescribed shape for the PSD would bias the estimate as the shape of the PSD would have limited degrees of freedom.

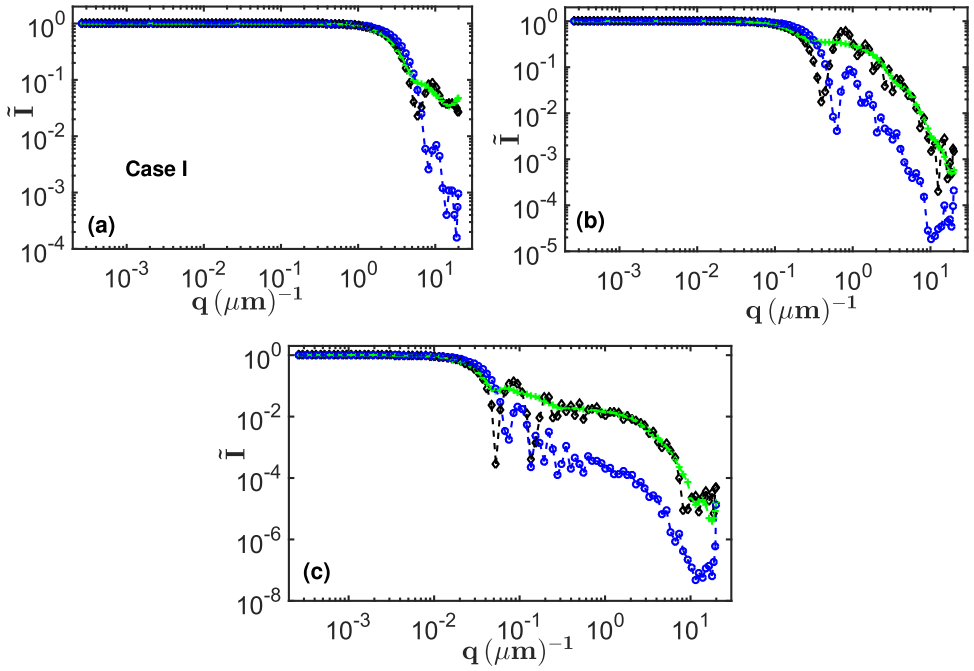

Fig. 3. Comparison of normalised scattering intensity patterns for needle-like and spherical particles of various sizes. Black diamonds: calculated scattering intensities for monodisperse needle-like particles with circular cross-section diameter of (a) $\overline{D}$ = 1 μm, (b) $\overline{D}$ = 10 μm and (c) $\overline{D}$ = 100 μm for Case I. Green crosses: best fit (using the scattering model for a multimodal distribution of spherical particles) to the scattering intensity of monodisperse needle-like particles obtained by solving the optimisation problem in Eq. (6). Blue circles: calculated scattering intensities for monodisperse spherical particles with diameter of (a) $\overline{D}$ = 1 μm, (b) $\overline{D}$ = 10 μm and (c) $\overline{D}$ = 100 μm. The needle-like particles were modelled as infinitely long cylinders. (For interpretation of the references to color in this figure caption, the reader is referred to the web version of this paper.)

then it is used to estimate the volume based PSD X_i^v as described in Section 2 of the supplementary information. Finally, the volume based PSD is normalised as

$$\widehat{X}_i^v = \frac{X_i^v}{\sum_{i=1}^N X_i^v} \tag{9}$$

where $\widehat{X}_i^v$ is the volume fraction of spherical particles of size $\overline{D}_i$.

3.2. Mean particle size

The mean size of the particles in a population can be represented by various metrics depending on the application (Merkus, 2009). The volume weighted mean diameter D_{43} is commonly reported by commercial laser diffraction instruments. The D_{43} value is defined as Merkus (2009)

$$D_{43} = \frac{\sum_{i=1}^N X_i \overline{D}_i^4}{\sum_{i=1}^N X_i \overline{D}_i^3}, \tag{10}$$

which upon using the substitution $X_i^v = X_i v_i$ (where v_i is the volume of the spherical particle with diameter $\overline{D}_i$) becomes

$$D_{43} = \sum_{i=1}^N \widehat{X}_i^v \overline{D}_i, \tag{11}$$

The D_{43} value will coincide with the diameter of spherical particles in a monodispersed population.

4. Results and discussion

Suspended needle-like particles experience various kinds of flow conditions depending on the vessel shape, agitation arrangement, solid loading and so on. Depending on these conditions, the particles may be able to perform completely random or partially restricted rotations or they could become fully aligned with the flow field. Flow-through cells typically used in laser diffraction instruments are a few millimetres wide where the incident laser beam is perpendicular to the flat transparent windows enclosing the cell and to the direction of flow through the cell. Depending on the shape, size and solid loading of particles, their rotations in such flow through cells may be restricted and in the limit of thin needles or thin platelets at high solid loadings they can become fully aligned with the flow with their main axis being perpendicular to the incident laser beam. Motivated by this, we consider two limiting cases: case I, where the incident beam is perpendicular to the main axis of the particle, and case II, where the incident beam is at a random angle to the main axis of the particle. These two cases will be examined in detail below.

When the particles are free to perform random rotations, the incident angle of the incoming monochromatic light will take all possible values from grazing to normal incidence with equal probability. However, when the particles are aligned with the flow field, the incident laser beam will be perpendicular to the particle main axis and hence the incident angle is fixed at 90° (see Fig. 1 of the supplementary information for a schematic for light scattering by an infinitely long cylinder).

The refractive indices of materials typically encountered in organic crystals (e.g., in pharmaceutical manufacturing) are around N_r=1.50 with zero absorption. For example, the cellobiose octaacetate, benzoic acid and metformin hydrochloride crystals shown in Fig. 1 have refractive indices of N_r = 1.51, 1.50 and 1.58 respectively. The three materials have poor solubility in methanol which has a refractive index N_r=1.33. Hence the refractive index of N_r=1.50 was used in the simulation of the scattering intensities of needle-like particles (modelled as infinitely long cylinders), and the particles were assumed to be suspended in a non-solvent medium with refractive index N_r=1.33. The wavelength of the incident light was fixed at λ = 0.633 μm in all the calculations which is consistent with the wavelength of red light in typical commercial laser diffraction instruments.

4.1. Case I: restricted rotations

The calculated scattering intensities for monodisperse needle-like particles with the diameter of circular cross-section of $\overline{D}$ = 1 μm,

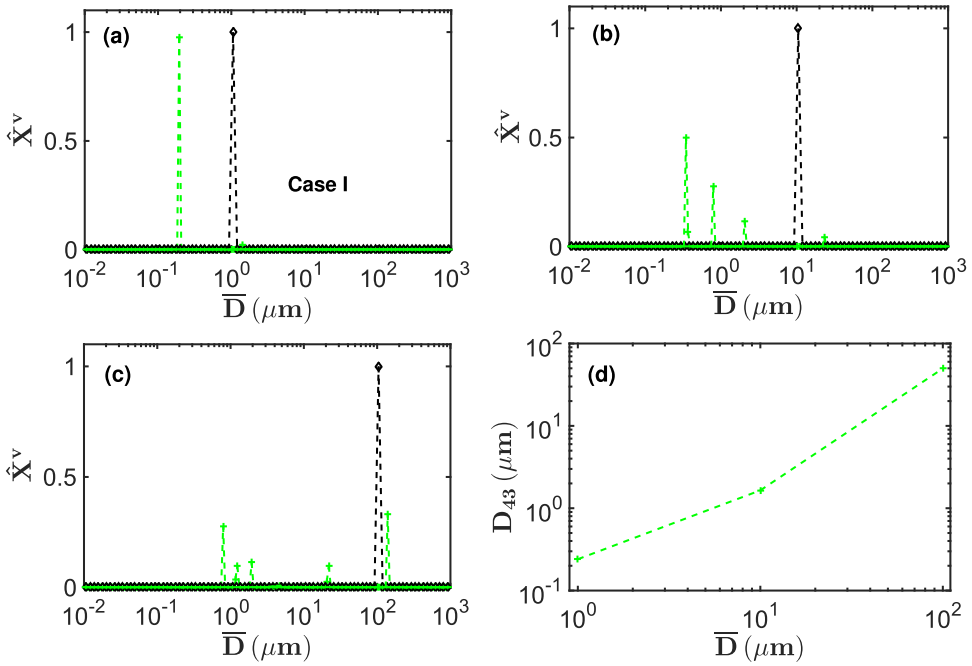

Fig. 4. Comparison of simulated and estimated size distributions. Black diamonds: monodisperse distributions of circular cross-sectional diameters for needle-like particles of (a)$\overline{D}$ = 1 μm, (b)$\overline{D}$ = 10 μm and (c)$\overline{D}$ = 100 μm for Case I. Green crosses: multimodal volume based distributions of diameters of spherical particles which give the best fit to the scattering intensities (shown in Fig. 3) of the needle-like particles whose distribution of cross-sectional diameters are shown by the black diamonds in (a), (b) and (c). The best fits are obtained by solving the optimisation problem in Eq. (6) with the spherical model. (d)D_{43} values estimated from the volume based PSDs obtained with the spherical model. The needle-like particles were modelled as infinitely long cylinders. (For interpretation of the references to color in this figure caption, the reader is referred to the web version of this paper.)

10 μm, and 100 μm are shown in Fig. 3 (black diamonds). The blue circles in Fig. 3 show the calculated scattering intensity for monodisperse spherical particles with diameter equal to the diameter of circular cross-section of needle-like particles. It can be seen in Fig. 3(a) that for $\overline{D}$ = 1 μm both scattering patterns are quite similar for lower q values, while in the high q ($q \gtrsim 5\ \mu m^{-1}$) region the scattering intensity for spheres is much lower than that for the needle-like particles. However, we can see that the scattering intensity pattern for monodisperse needle-like particles can be reasonably well fitted using scattering from a multimodal distribution of spherical particles. The fitted curve shown by the green crosses in Fig. 3(a) is obtained by solving the optimisation problem in Eq. (6).

In order to quantify the degree of fit, we compute the L_2 norm (L_2^{fit}) of the difference between the scattering intensities of the needle-like particles (modelled as infinitely long cylinders) and that of the fitted curve from the spherical model. This gives $L_2^{fit} = 0.142$. This value is nearly one third of the L_2 norm (L_2^{sphere}) of the difference between the scattering intensities of the needle-like particles and that of the spherical particles whose diameters are equal to those of the circular cross-sectional diameter of the infinitely long cylinder. The value of L_2^{sphere} is 0.415 for the case of $\overline{D}$ = 1 μm.

The multimodal PSD (in terms of volume fractions $\hat{X}^v$) of spherical particles is shown in Fig. 4(a). In order to achieve a reasonable fit (quantified by the L_2^{fit} value), the estimated PSD needs to contain at least two modes, with 98% (by volume) of particles with diameter ≈0.2 μm and 2% (by volume) of particles with diameter ≈1.4 μm. This can be understood by considering the difference in shapes between scattering patterns of spheres and thin cylinders.

In the low q region, the normalised scattering intensity $\tilde{I}$ is independent of q regardless of particle shape. In the Guinier region, the scattering intensity starts decreasing with increasing q and can be approximated as $\tilde{I}(q)/\tilde{I}(0) = 1 - q^2R_g^2/3$ (Sorensen and Shi, 2000), where R_g is the radius of gyration of the particles and $\tilde{I}(0)$ is the zero q limit of $\tilde{I}$ which is indicated as I_1 in Eq. (4). The Guinier region extends towards $qR_g \approx 1$ where a noticeable downturn of the scattering intensity can be observed. For spherical particles $R_g = \overline{D}\sqrt{(3/20)}$ so that the downturn in the scattering intensity can be seen when $q \approx (2/\overline{D})\sqrt{(5/3)}$ (i.e., at $q \approx 3\ \mu m^{-1}$ for $\overline{D}$ = 1 μm). At large q values the scattering intensity transits into the Porod region where it decays with an exponent depending on the nature of the particle surface (for smooth surfaces $\tilde{I} \sim q^{-4}$ Sorensen, 2001).

It can be seen in Fig. 3(a) that the scattering intensity pattern for the monodisperse needle-like particles (modelled as infinitely long cylinders) of circular cross-sectional diameter $\overline{D}$ = 1 μm (black diamonds) turns down at slightly lower q values than for spheres of the same diameter. Therefore a slightly larger sphere diameter is needed to reproduce the Guinier region of a thin cylinder and the estimated PSD (green crosses in Fig. 4(a)) contains a peak at a particle diameter slightly larger than 1 μm. The scattering intensity pattern for thin cylinders of circular cross-sectional diameter $\overline{D}$ = 1 μm initially decays faster than that of spheres of the same diameter at higher q values (Fig. 3(a)). However, the decrease of the scattering intensity pattern for the thin cylinders slows down considerably as q increases, whereas the corresponding scattering intensity for spheres continue to decrease with increasing q. Hence, the scattering pattern of a thin cylinder cannot be fitted with just that of a single sphere. In order to get a reasonable fit (judging by the L_2^{fit} value), it is necessary to include additional scattering at larger q values, which can only come from much smaller spherical particles and the resulting PSD will become multimodal. This can be seen as a second peak at $\overline{D} \approx 0.2$ μm in the estimated PSD in Fig. 4(a). This peak is a pure artefact in the estimated PSD as it does not correspond to any physical length scale related to the particle size and arises solely from the difference of scattering patterns between cylinders and spheres. The same phenomenon can be seen for other cylinder sizes as shown in Figs. 3(b) and 4(b) (for circular cross-section diameter of $\overline{D}$ = 10 μm and $L_2^{fit} = 0.828$, $L_2^{sphere} = 1.318$) and Figs. 3(c) and 4(c) (for circular cross-section diameter of $\overline{D}$ = 100 μm and $L_2^{fit} = 0.181$, $L_2^{sphere} = 0.521$). The consequence of these artificial particle size modes are the grossly under-estimated D_{43} values for the respective particle sizes as seen in Fig. 4(d).

To further understand that using the spherical model requires a multimodal PSD to fit the scattering intensity of the needle-like

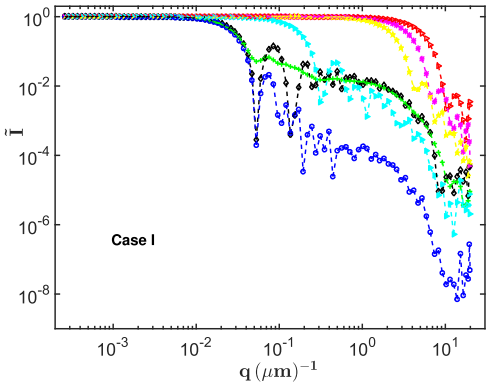

Fig. 5. Calculated scattering intensities for monodisperse populations of spherical particles of diameters $\overline{D}$ = 0.8 μm (red triangles), $\overline{D}$ = 1.2 μm (magenta filled symbols), $\overline{D}$ = 1.9 μm (yellow pentagrams), $\overline{D}$ = 21 μm (cyan filled triangles) and $\overline{D}$ = 140 μm (blue circles). The green crosses are the superposition of the corresponding scattering intensities (weighted by the number fractions estimated from the volume fractions shown by the green crosses in Fig. 4(c)). The black diamonds are the scattering intensity for needle-like particles of circular cross-sectional diameter $\overline{D}$ = 100 μm. The needle-like particles were modelled as infinitely long cylinders. (For interpretation of the references to color in this figure caption, the reader is referred to the web version of this paper.)

particles, consider the case of the scattering intensity of needle-like particles (modelled as infinitely long cylinders) with circular cross-sectional diameter $\overline{D}$ = 100 μm shown by the black diamonds in Fig. 5. The PSD estimated by fitting (solving the optimisation problem in Eq. (6)) the spherical model to this scattering intensity contains major peaks at $\overline{D}$ = 0.8 μm, $\overline{D}$ = 1.2 μm, $\overline{D}$ = 1.9 μm, $\overline{D}$ = 21 μm and $\overline{D}$ = 140 μm as shown by the green crosses in Fig. 4(c). A scattering intensity corresponding to the fitted curve shown by the green crosses in Fig. 3(c) can be constructed by performing a superposition of the scattering intensities for monodisperse spherical particles of sizes $\overline{D}$ = 0.8 μm, $\overline{D}$ = 1.2 μm, $\overline{D}$ = 1.9 μm, $\overline{D}$ = 21 μm and $\overline{D}$ = 140 μm shown in Fig. 5.

The superposition is performed by weighting the scattering intensities by their respective number fractions estimated as $\widehat{X}_s = \widehat{X}_s^v/\overline{D}_s^3$ where subscript s represents particle size and $\widehat{X}_s^v$ is the volume fraction corresponding to each size as shown in Fig. 4(c). The normalised scattering intensity obtained by this superposition procedure is shown by the green crosses in Fig. 5, and it has a good fit (L_2^{fit} = 0.182) to the original scattering intensity (black open diamonds in Fig. 5) for the needle-like particles (modelled as infinitely long cylinders) of circular cross-sectional diameter $\overline{D}$ = 100 μm. This fit cannot be obtained if the weighted scattering intensities from the smaller particle sizes of $\overline{D}$ = 0.8 μm, $\overline{D}$ = 1.2 μm, $\overline{D}$ = 1.9 μm and $\overline{D}$ = 21 μm are not included in the superposition.

4.2. Case II: random rotations

Case II where the needle-like particles are able to make random rotations is analysed in this section. As in Case I, the scattering intensity pattern of the needle-like particles will be simulated with the model for infinitely long cylinders, while the inverse problem will be solved with the model for spherical particles. In this case, the scattering intensities are computed for various values of incident angle from 1° to 90°. Then the overall scattering intensity is obtained by averaging these scattering intensities over all angles.

Compared to Case I, the Guinier region of the scattering intensity (blue circles in Fig. 6) for spherical particles of diameter $\overline{D}$ = 1 μm matches that of needle-like particles (black diamonds in Fig. 6) of the same circular cross-sectional diameter much more closely. This leads the spherical model to estimate the largest particle size with the diameter which is very close to the circular cross-sectional diameter of the needle-like particles (modelled as infinitely long cylinders) as shown by the green crosses in Fig. 7. However, similar to Case I, the decay of the scattering intensity pattern for needle-like particles slows down at higher q values when compared with those of spheres of the same cross-sectional diameter as seen in Fig. 6. Hence as in Case I, in order to get a reasonable fit (based on the L_2^{fit} value), it is necessary to include additional scattering at larger q values, which must come from particles with much smaller diameters and the resulting PSD thus

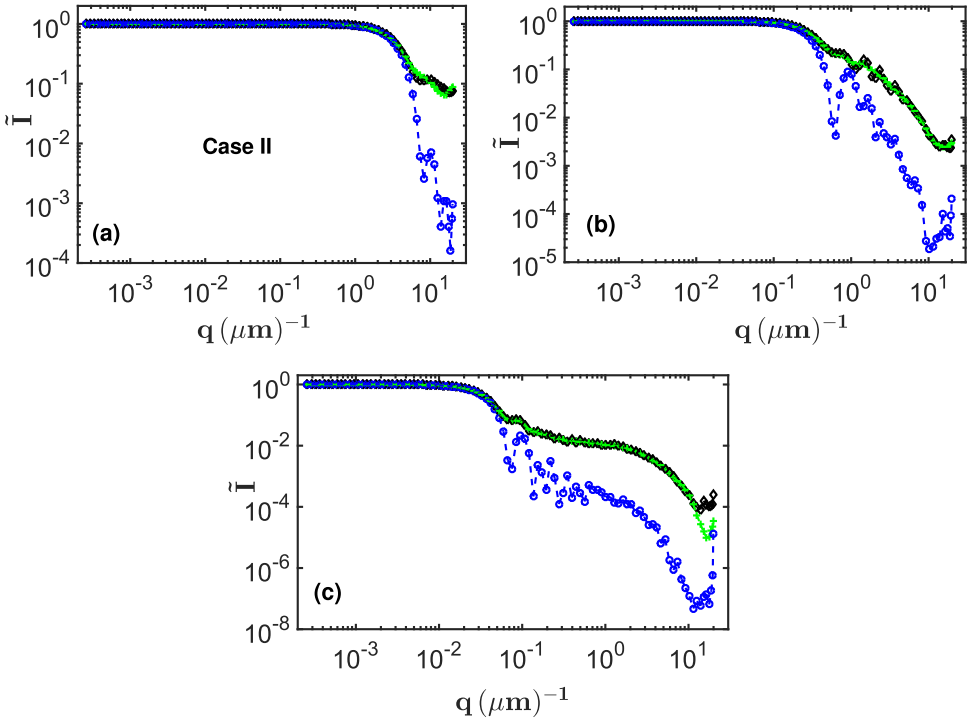

Fig. 6. Comparison of normalised scattering intensity patterns for needle-like and spherical particles of various sizes. Similar to Fig. 3 but for Case II. (For interpretation of the references to color in this figure caption, the reader is referred to the web version of this paper.)

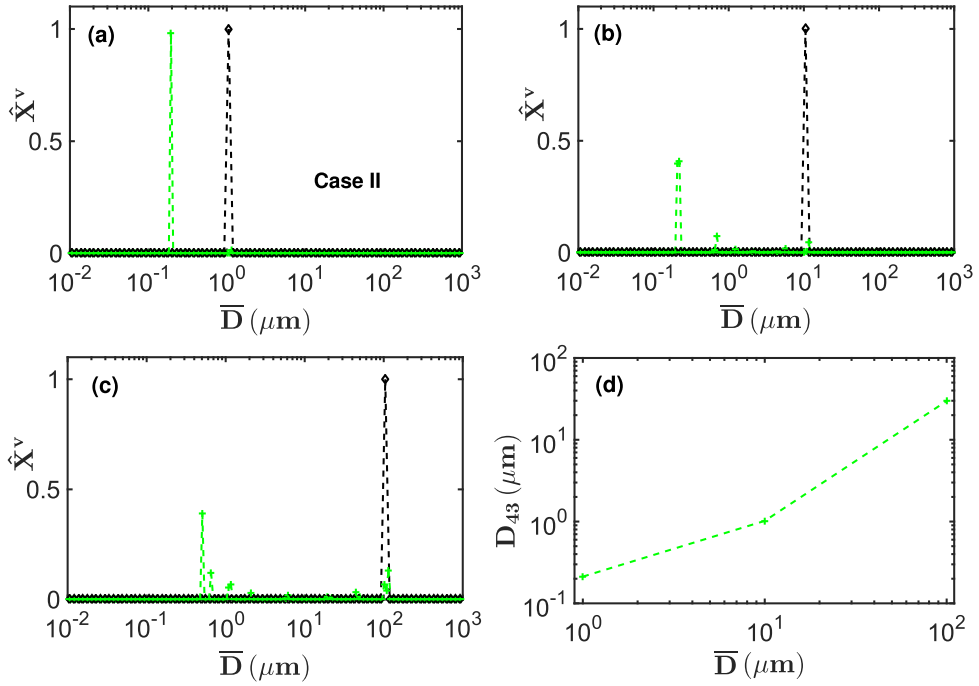

Fig. 7. Multimodal volume based distributions of diameter of spherical particles corresponding to best fits of scattering patterns of monodisperse needle-like particles. Similar to Fig. 4 but for Case II. (For interpretation of the references to color in this figure caption, the reader is referred to the web version of this paper.)

become multimodal, although the smaller size peaks are artefacts in the estimated PSD. As before, the consequence of these additional peaks introduced into the estimated PSD by the spherical model is that the estimated D_{43} values can be significantly lower that the actual cross-sectional diameter of needle-like particles as seen in Fig. 7(d).

5. Conclusions

We have demonstrated the origin of artefacts which arise due to applying a model for scattering by spherical particles to solve the inverse problem for laser diffraction when the scattering intensity pattern comes from a population of needle-like particles. The scattering intensity patterns for the needle-like particles were simulated with the model for infinitely long cylinders using a monodisperse distribution (in terms of the circular cross-sectional diameters) of these cylinders. Our results show that using the scattering model for spherical particles it is possible to find a good fit for the scattering intensity patterns of needle-like particles, but the resulting estimated PSD is not necessarily representative of actual cross-sectional diameters of the needle-like particles. The estimated PSDs are typically multimodal with the largest size mode close to the actual cross-sectional diameter but additional smaller size modes are not physical. These modes are mathematical artefacts arising from different shapes of scattering patterns of spheres and thin cylinders. Needle-like particles of various lengths would be expected to give rise to similar effects which would depend on the aspect ratio of the particles. It can be expected that the same issue applies for particles of other shapes, such as platelets.

This situation is unavoidable as long as the scattering model for spherical particles is used to fit the data from particles of strongly non-spherical shapes as it is possible to fit essentially any scattering pattern with the scattering models for a polydiperse population of spheres. This approach is used in commercial laser diffraction instruments, and it can lead to misleading conclusions about the PSD of the particles under analysis, in terms of unrealistic multimodal distributions and under-estimating the mean particle size in terms of volume weighted mean diameter values. Therefore, the way forward is to obtain information about particle shape and apply appropriate scattering models for particles to be analysed.

Acknowledgements

This work was performed within the UK EPSRC funded project (EP/K014250/1) ‘Intelligent Decision Support and Control Technologies for Continuous Manufacturing and Crystallisation of Pharmaceuticals and Fine Chemicals’ (ICT-CMAC). The authors would like to acknowledge financial support from EPSRC, AstraZeneca and GSK. The authors are also grateful for useful discussions with industrial partners from AstraZeneca, GSK, Mettler-Toledo, Perceptive Engineering and Process Systems Enterprise. The authors also wish to thank Thomas McGlone and Vaclav Svoboda for providing the images in Fig. 1.

Appendix A. Supplementary data

Supplementary data associated with this article can be found in the online version at http://dx.doi.org/10.1016/j.ces.2016.10.031.

References

Washington, C., 1992. Particle Size Analysis in Pharmaceutics and Other Industries. Ellis Horwood Limited, Chichester, England.
Shekunov, B.Y., Chattopadhyay, P., Tong, H.H.Y., Chow, A.H.L., 2007. Particle size analysis in pharmaceutics: principles, methods and applications. Pharm. Res. 24 (2), 203–227.
Abbireddy, C.O.R., Clayton, C.R.I., 2009. A review of modern particle sizing methods. Geotech. Eng. 162, 193–201.
Black, D.L., McQuay, M.Q., Bonin, M.P., 1996. Laser-based techniques for particle-size measurement: a review of sizing methods and their industrial applications. Prog. Energy Combust. Sci. 22, 267–306.
Bohren, C.F., Huffman, D.R., 1983. Absorption and Scattering of Light by Small Particles. John Wiley and Sons, Inc., Hoboken, United States.
Hamilton, P., Littlejohn, D., Nordon, A., Sefcik, J., Slavin, P., 2012. Validity of particle size analysis techniques for measurement of the attrition that occurs during vacuum agitated powder drying of needle-shaped particles. Analyst 137, 118–125.
Polakowski, C., Sochan, A., Bieganowski, A., Ryżak, M., Földényi, R., Tóth, J., 2014. Influence of the sand particle shape on particle size distribution measured by laser diffraction method. Int. Agrophys. 28, 195–200.
Wickramasinghe, N.C., 1973. Light Scattering Functions for Small Particles with Applications in Astronomy. Adam Hilger Ltd., London, United Kingdom.
Sorensen, C.M., 2001. Light scattering by fractal aggregates: a review. Aerosol Sci. Technol. 35 (2), 648–687.
Mishchenko, M.I., Hovenier, J.W., Travis, L.D., 2000. Concepts, terms, notation. In: Mishchenko, M.I., Hovenier, J.W., Travis, L.D. (Eds.), Light Scattering by Nonspherical Particles: Theory, Measurements and Applications. Academic Press, London, United Kingdom, 1–28, [Ch. 1].

Boyd, S., Vandenberghe, L., 2004. Convex Optimization. Cambridge University Press, Cambridge, UK.
Schenk, M., Thumann, A., Seeger, T., Leipertz, A., 1998. Pure rotational coherent anti-Stokes Raman scattering: comparison of evaluation techniques for determining single-shot simultaneous temperature and relative N_2-O_2 concentration. Appl. Opt. 37 (24), 5659–5671.
Aster, R.C., Borchers, B., Thurber, C.H., 2013. Parameter Estimation and Inverse Problems. Elsevier Inc., Amsterdam, The Netherlands.
Merkus, H.G., 2009. Particle size measurements fundamentals, practice, quality. Springer Science & Business Media B.V., Dordrecht, The Nertherlands.
Sorensen, C.M., Shi, D., 2000. Guinier analysis for homogeneous dielectric spheres of arbitrary size. Opt. Commun. 178, 31–36.